#### CONFERENCE PRE-PRINT

# REGIME OF ELECTRON INTERNAL TRANSPORT BARRIER IN HIGH-DENSITY NBI HEATED PLASMAS OF HELIOTRON J

S. KOBAYASHI, S. INAGAKI, K. NAGASAKI, S. OHSHIMA, T. MINAMI, S. KADO, F. KIN, S. INAGAKI, A. IWATA, S. KONOSHIMA, T. MIZUUCHI

Institute of Advanced Energy, Kyoto Univ., Uji, Kyoto Japan

Email: kobayashi@iae.kyoto-u.ac.jp

C. WANG, Y. NAKAMURA, R. MATSUTANI, A. MIYASHITA, A. MATSUYAMA,

Graduate School of Energy Science, Kyoto University, Uji, Kyoto, Japan

## P. ADULSIRISWAD

Rokkasho Fusion Institute, National Institute for Quantum Science and Technology, Rokkasho, Aomori, Japan

#### Y. SHIRASAWA, T. TATSUNO

The University of Electro-Communications, Chofu, Tokyo, Japan

#### M. YOSHIKAWA

Plasma Research Center, University of Tsukuba, Tsukuba, Ibaraki, Japan Town/City, Country

#### N. KENMOCHI

National Institute for Fusion Science, Toki, Gifu, Japan

In this work, we demonstrate a reduction in core electron heat transport and an improvement in global energy confinement observed in simultaneous formation of electron internal transport barrier (ITB) and edge transport barrier (ETB) in high-density NBI plasmas of Heliotron J. The high-density ( $n_e \sim 8 \times 10^{19} \,\mathrm{m}^{-3}$ ) electron ITB plasma is produced by introducing high-intense gas puffing (HIGP) at the magnetic field strength B = 1.4 T and by controlling the plasma current using balanced NB. Under the condition, a steep electron temperature gradient at the core region and a peripheral steep density (n<sub>e</sub>) gradient are observed at the same time with a transition to H-mode, resulting a simultaneous improvement in the core electron heat transport and global energy confinement exceeding the international stellarator/heliotron scaling (ISS04) law. In some cases, a high  $T_i$  gradient at the core region is observed as well. The operational regime of the high-density ITB plasmas is 50 times higher normalized collisionality (plateau regime) than that of conventional e-ITB (1/v regime) observed in low-density and high-power ECH plasmas. A different ITB formation mechanism to that of the conventional e-ITB is expected because (1) dynamics of the high-density ITB formation has a time scale of the energy confinement time and (2) negative radial electric field  $E_r$  is predicted by a neoclassical (NC) transport calculation. The position of the ITB foot (r/a = 0.3) coincides with both the parallel flow velocity shear and the m/n = 7/4 rational surface deduced by HINT2 code. A gyrokinetic simulations using GX code reveals that the turbulent potential fluctuations in the ion temperature gradient (ITG) mode are more stretched along with the magnetic field line when the magnetic shear becomes low expected by the rotational transform profile with HINT2, compared to configurations with magnetic shear implied by observed pressure gradients. It implies that nonlinear eddy selfinteractions around the rational surface may cause the parallel flow shear, resulting in reduction of the heat transport.

# 1. INTRODUCTION

In order to establish reactor relevant conditions in magnetically confined fusion plasmas, it is required to achieve compatibility between core improved confinement and edge high density conditions. Research on the coexistence of internal transport barrier (ITB) and edge transport barrier (ETB) have been conducted in Tokamaks [1, 2]. Under high- $\beta_p$  operation in DIII-D, formation of an internal transport barrier (ITB) with an H-factor exceeding 1.5 have been confirmed in high-density H-mode plasmas which exceeds the Greenwald density limit by over 10%. In JT-60U tokamak, experimental conditions for the coexistence of ITB and H-mode plasmas have been studied in the high- $\beta_p$  operation [3]. It has been reported the control of the magnetic shear and low order rational surface has been a key factor for achieving the high-performance plasmas [4–7]. Therefore, experimental clarification for the relationship between the magnetic shear and the transport barriers is a common issue in Tokamak and Stellarator/Heliotron devices.

In the Stellarator/Heliotron configurations, on the other hand, the density operation regimes for the electron internal transport barrier (ITB) formation have been limited because it has been strongly connected to the transition to Core Electron-Root Confinement (CERC) with a positive neoclassical (NC) radial electric field which

is obtained by strong electron cyclotron heating (ECH) in relatively low density plasmas around 1×10<sup>19</sup> m<sup>-3</sup> [8–12]. The ion ITB formation or improvement in the ion heat transport in the Stellarator/Heliotron devices have been reported in LHD and W7-X. In the deuterium plasmas of LHD, high ion temperature exceeding 10keV has been achieved with high electron temperature conditions by superimposed ECH into neutral beam injection (NBI) heating [13, 14], while the electron density has been around 1×10<sup>19</sup> m<sup>-3</sup> with no H-mode transition. An improvement in the ion heat transport has been found in W7-X using continuous pellet injection in strong ECH plasmas [15]. The gyrokinetic simulation has revealed that a peaked density profile and a negative radial electric field had an effect to reduce the ion temperature gradient (ITG) mode in the post-pellet phase. These discharges have been reported the improvement in the ion heat transport, but it has not been realized the ITB formation in conjunction with ETB associated with the H-mode transition. Therefore, the development of the operational scenarios for the high-density ITB formation is indispensable to realizing Heliotron-type reactor. The H-mode study in CHS has revealed that the considerable increase in the electron temperature with electron ITB in the core region has been observed with the ETB formation for several specific discharges [16, 17]. Although the electron temperature has reached up to 0.7 keV at the core, further experiment and analysis including the electron transport have not been conducted.

Our recent research has demonstrated that e-ITB was formed in the NBI sustained plasmas of Heliotron J [18]. The peaked electron temperature with steep temperature gradient at the core was formed with the core electron density around  $2\times10^{19}$  m<sup>-3</sup> by high-intensity gas puffing (HIGP) method. The HIGP method [19, 20] enabled an efficient particle fuelling by applying short-pulsed ( $10\sim15$  ms) and strong gas puffing, while suppressing peripheral hydrogen recycling. The neoclassical transport calculation revealed that a different e-ITB formation mechanism to that of the conventional e-ITB case has been expected because negative radial electric field  $E_r$  was predicted whole the confinement region. Using the fuelling method, H-mode transition has also been observed in Heliotron J [19]. The radial electric field based on the poloidal charge exchange recombination spectroscopy (CXRS) indicates the formation of a large  $E_r$  shear of -250 kV/m<sup>2</sup> in the peripheral region [21], which has been considered to be contribute to turbulence suppression. Therefore, it has been desired that the development of an operational method which achieves the compatibility between the ITB and ETB.

In this study, we demonstrate the high density NBI plasmas of Heliotron J which has both electron/ion ITB and ETB. The experimental setup is presented in the next section. The operational method for the high-density plasmas using HIGP will be explained followed by experimental observations in section 3. A candidate mechanism for the ITB formation will be discussed in section 4. Finally, the summary is presented in section 5.

#### 2. EXPERIMENTAL SETUP

Heliotron J is a medium-sized ( $\langle R_0 \rangle / \langle a_p \rangle = 1.2 \text{m}/0.17 \text{m}$ ) helical-axis heliotron device with an L=1 four-period helical winding coil, where  $R_0$  and  $a_p$  are major radii and L is pole number, respectively. Figure 1 shows a schematic illustration of Heliotron J. The plasma volume is 0.68 m³ in the standard configuration of Heliotron J. Two tangential NBI systems (BL1 and BL2) have a maximum beam power of 0.7 MW each and an acceleration voltage of 30 keV. Hydrogen gas is used in the ion source of NBI, while deuterium gas is used for the plasma fuelling. The gas fuelling is controlled by four-sets of pre-programmed Piezo-electric valves located at inner side of each toroidal section. Therefore, toroidally uniform and effective gas fuelling could be achieved in this system.

In this study, we used an initiation method for the NBI target plasmas using non-resonant 2.45 GHz microwave [22-24]. The initiation technique enabled the NBI plasma start-up regardless of resonant condition even at low NBI power (> 0.3 MW), low acceleration voltage (< 30 kV) and small device size (~ 1 m).

#### 3. EXPERIMENTAL RESULTS

### 3.1. ITB plasma formation in high-density NBI plasmas

In this study, we carried out ITB plasma discharge experiments in the standard configuration of Heliotron J by changing the magnetic field strength from B = 0.8 to 1.4 T to find the operational regime of the electron ITB formation. The

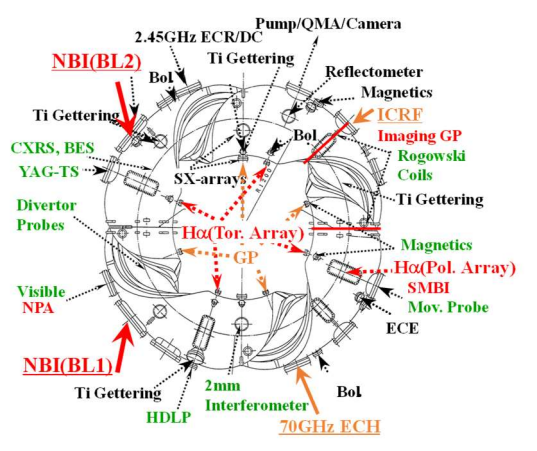


FIG. 1. Schematic illustration of Heliotron J.

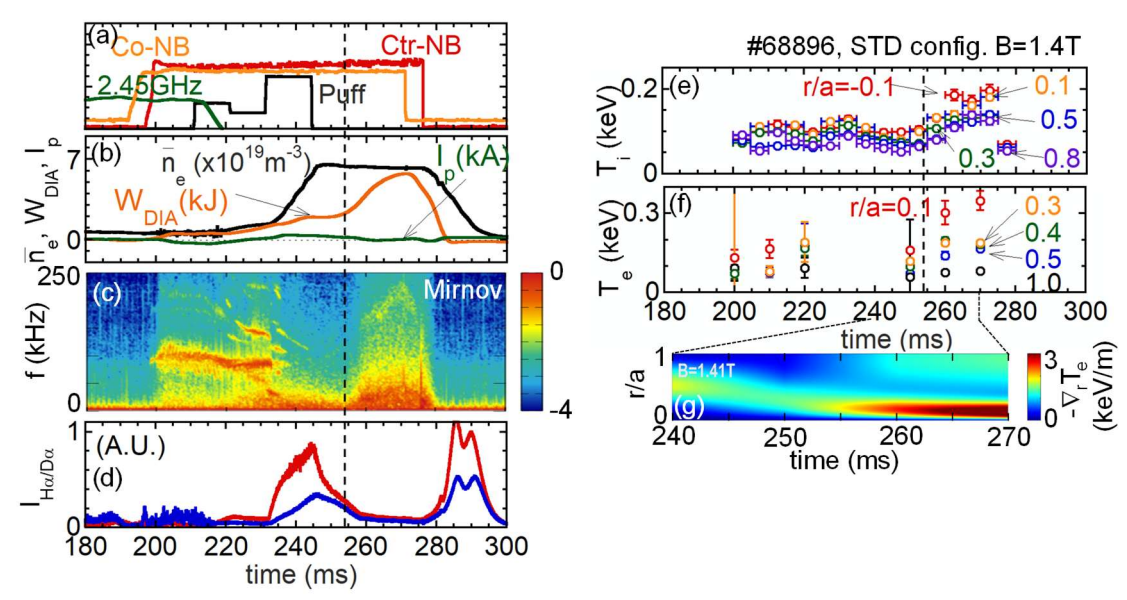


Fig. 2. Time evolution of heating, fuelling and plasma parameters obtained in high-density ITB plasmas.

rotational transform profile in the vacuum condition of the standard configuration has quite low magnetic shear just below the m/n = 7/4 rational surface, which will be shown later. As shown in Fig. 2, the plasma was heated only by balanced NB (co-NB: 0.3MW, ctr-NB: 0.3MW) with assistance of the pre-ionization using 2.45 GHz microwave. A high-density plasma with the line-averaged electron density  $\bar{n}_e \sim 7 \times 10^{19} \text{ m}^{-3}$  was achieved by HIGP with pulse timing of t = 230-245 ms. The H<sub> $\alpha$ </sub>/D<sub> $\alpha$ </sub> line emission intensity close to the piezoelectric valve shows a strong external fuelling was applied. After the stop of the HIGP fuelling, on the other hand, the reduction in hydrogen recycling was observed by the  $H_0/D_a$  measurement, which contributed to controlling the charge exchange and radiation loss. An H-mode transition occurred associated with a drop of the  $H_{\alpha}/D_{\alpha}$  line emission intensity at t = 254 ms, after that, a remarkable recovery of the stored energy and a slightly increase in the electron density was observed despite no external gas fuelling. The recovery of the stored energy has been observed in Heliotron J after the injection of the ice pellet [25]. During the discharge, the plasma current was almost zero due to the balanced NB injection. From the beam power absorption analysis [26], the energy confinement time is 19 ms at t = 260 ms, which exceeds 20% of the international stellarator scaling (ISS04) law [27]. The energy confinement time and the heat transport will be discussed later. The magnetic probe signals before HIGP show several modes regarding as fast ion induced MHD instabilities. In the recovery phase, on the other hand, a broad band fluctuation was observed with a high frequency peak around f = 200kHz. The auto-bicoherence analysis for the broadband fluctuations indicates that no three-wave interactions are confirmed. Although, the broadband fluctuations have not been identified yet, further analysis will be carried out using MHD or gyrokinetic simulations.

The time evolution of the electron temperature (T<sub>e</sub>) represents a dynamic movement of the  $T_e$  gradient  $-\nabla_r T_e$  during and after HIGP. As shown in Fig. 2(g), the high T<sub>e</sub> gradient region moves from middle position  $(r/a \sim 0.5)$  to the plasma core with a time scale of the energy confinement time (~20 ms). Finally, the formation of electron ITB with a steep  $T_e$  gradient was seen at t =260 ms with the peak  $T_{\rm e}$  of 0.35keV. This experimental observation indicates that the dynamics of the high-density ITB formation differ from that of the conventional e-ITB formation which is characterized by the CERC transition represented by a fast change from negative (ion-root)  $E_r$  to positive (electron-root)  $E_r$ . The carbon ion temperature measured with CXRS [28]

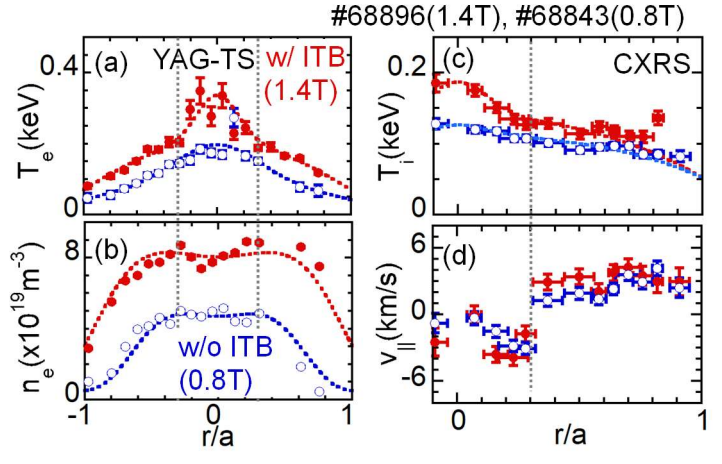


Fig. 3. Radial profile of (a) electron temperature, (b) electron density, (c) ion temperature and (d) parallel flow velocity for B = 1.4 (closed circles) and 0.8 T (open circles) cases.

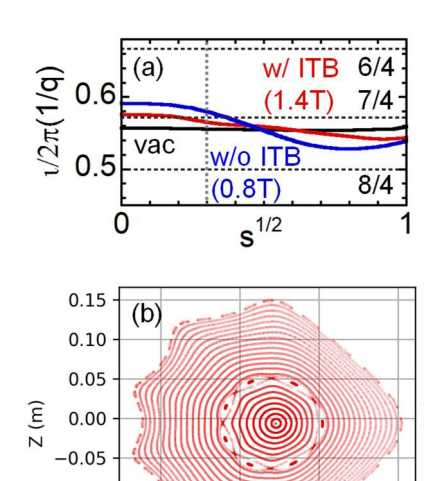
shows not only the core ion temperature at r/a = -0.1 and 0.1 but also the peripheral ion temperature at r/a = 0.8 increased as well during the recovery phase.

The radial profile of the electron density, electron temperature, ion temperature and parallel flow velocity are plotted in Fig. 3 as a comparison between ITB (B = 1.4 T) and no-ITB cases (B = 0.8 T). In both the cases, the radial profiles are compared at the timing where the maximum stored energy was obtained. Clear electron ITB was observed for the B = 1.4 T case. Almost the flat or slightly hollow density profile can be seen inside the ITB, while a steep density gradient was formed at the peripheral (|r/a| > 0.7) region, which has been commonly observed in the H-mode plasmas of Heliotron J. Note that a strong shear in the parallel flow velocity was measured at the same position as the footpoint of the electron ITB ( $r/a \sim 0.3$ ). In the no ITB case at B = 0.8 T, on the other hand, temperature profiles have no discontinuity in the electron temperature gradients near the plasma core, while the parallel flow velocity shear being relatively smaller than that of the ITB case was observed. The normalized collisionality  $v^*$  observed in the ITB plasmas is plateau regime, which is 50 times higher than that of the conventional e-ITB plasmas produced by ECH. These ITB characteristics are closer to those obtained in Tokamak plasmas rather than the conventional e-ITB in Stellarator/Heliotron plasmas.

#### 3.2. Equilibrium and transport analyses

Figure 4(a) shows the rotational transform profile calculated by VMEC fixed boundary equilibrium. For the vacuum case, the rotational transform profile has a quite low magnetic shear. The rotational transform increases in the core region and decreases in the peripheral region due to the plasma pressure effect. The VMEC equilibrium calculation indicates the existence of a low-order (m/n = 7/4) rational surface around  $r/a = 0.25 \sim 0.35$  for B = 0.8 and 1.4 T cases, which is consistent to the experimental observations that the parallel flow velocity shear was observed. Then the presence of rational surface and the flow shear might not be sufficient conditions for the ITB formation. The existence of the m/n = 7/4 rational surface is expected by the HINT2 free boundary equilibrium calculation as well. The rotational transform profile deduce by HINT2 has a quite low magnetic shear around the m/n= 7/4 island, whose size is calculated to be  $\sim 1$ cm at the O-point. The modification of the local magnetic shear by magnetic island may affect the viscosity and the turbulent transport through nonlinear interactions of turbulence, therefore the effect onto the ITB formation should be carefully discussed. This will be presented in the next section.

As shown in Fig. 5(a), the transport analysis using TASK-3D [29] reveals a strong reduction in the effective electron heat transport coefficients  $\chi_e^{\text{eff}}$  at the core region in the ITB case (B=1.4 T). The neoclassical transport analysis was carried to obtain the electron heat transport coefficient  $\chi_e^{\text{NC}}$  and the neoclassical radial electric field  $E_r^{\text{NC}}$  [30, 31]. The experimentally observed heat transport coefficient  $\chi_e^{\text{eff}}$  for the ITB case is about 1/8 of the no-ITB case, however, a difference from the neoclassical heat transport  $\chi_e^{\text{NC}}$  indicates a significant transport by turbulence still remains. A negative neoclassical radial electric field shown in Fig. 5(b) is expected in the confining regions because of the high collisionality. These characteristics differ from the conventional e-ITB formation associated with the CERC transition [8–12]. In the ion/electron ITB plasmas of the ECH superimposed NBI plasmas of



R (m)
Fig. 4. Radial profile of (a) rotational
transform for vacuum, B = 0.8 and 1.4 T
cases deduced by VMEC and (b) poincare
plot of magnetic flux surface for B = 1.4 T
case calculated by HINT2 code.

1.3

1.4

1.5

-0.10

-0.15

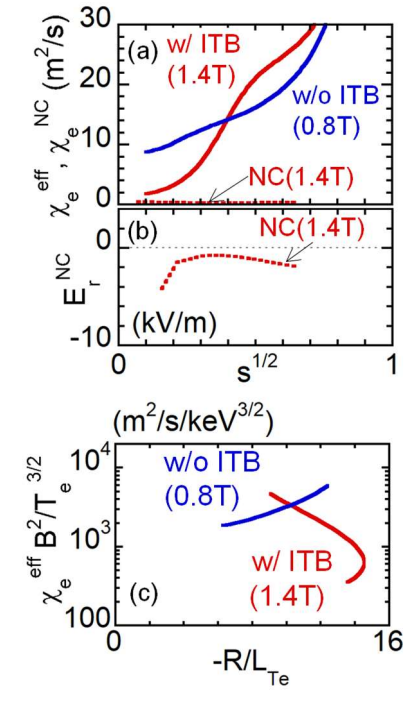


Fig. 5. Radial profile of (a) electron heat transport coefficient in case of B=0.8 and 1.4 T and that calculated by neoclassical transport analysis, (b) neoclassical radial electric field in case of B=1.4 T. The electron heat transport coefficient normalized by gyro-Bohm scaling is plotted in the radial location of 0.1 < r/a < 0.3 as a function of inverse scale length.

LHD, it has been reported that the improvements of the ion/electron heat transport depend on the ratio of electron to ion temperature  $T_o/T_i$  [32]. Basically, the characteristic of the turbulent transport (ITG/ETG/TEM) is affected by the  $T_o/T_i$  ratio as well as the magnetic shear. The  $T_o/T_i$  ratio observed in this study is approximately 2, and in addition, the magnetic shear is expected to be low in the Heliotron J configuration, further analysis is required regarding the relationship between ion and electron heat transport.

The transport characteristics of the ITB plasma were investigated by comparing the gyro-Bohm scaling. Figure 5(c) shows the effective electron heat transport coefficient  $\chi_{\rm e}^{\rm eff}$  in the radial location 0.1 < r/a < 0.3 normalized by the gyro-Bohm scaling factor  $(T_{\rm e}^{3/2}/B^2)$  as a function of the inverse scale length  $R/L_{\rm Te}$ , where R and  $L_{\rm Te}$  are the major radius of Heliotron J and the scale length of the  $T_{\rm e}$  profile. As compared with the no-ITB case, a reduction in the normalized transport coefficient by 1/10 is obtained in the case with ITB. Since the thermal diffusivity of the gyro-Bohm scaling is

expected as  $T_e^{3/2}/B^2$ , the electron heat transport coefficient of the ITB case is smaller than that predicted by the electron temperature dependence of the gyro-Bohm scaling, which is similar to that observed in the conventional e-ITB plasmas of Heliotron J [33].

#### 3.3. ITB dependence on magnetic field strength

The magnetic field scan experiments show the ITB formation depends on the magnetic field strength. Figure 6 shows the time evolution of the electron temperature gradient  $-\nabla_r T_e$  for the magnetic field strength from 0.8 T to 1.4 T cases. These experimental data were obtained with constant neutral beam power of 0.6MW in the balanced injection. Both the achieved

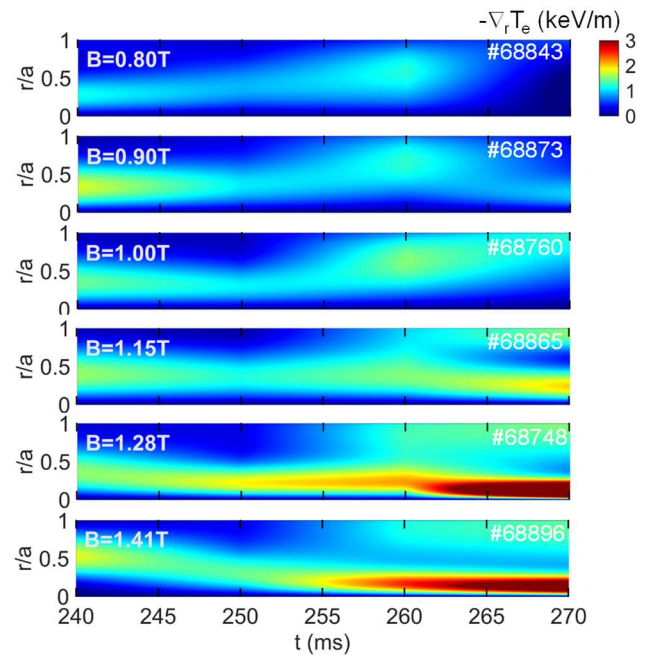


Fig. 6. Time evolution of electron temperature gradient for B= 0.8, 0.9, 1.0 1.15, 1.28 and 1.41 T cases, respectively. Electron ITB with steep  $T_e$  gradient can be seen for B > 1.28T.

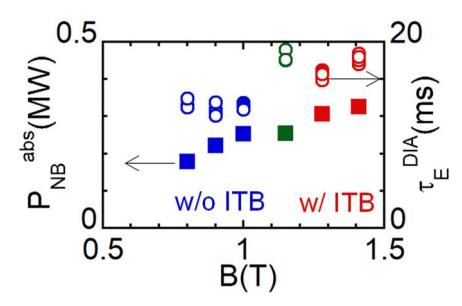


Fig. 7. Dependence of NBI absorption power and energy confinement time on magnetic field strength.

maximum density and electron temperature were increased with increase the magnetic field strength, then the normalized collisionality was kept within a factor of two during the magnetic field scan. In all the magnetic field strength, a relatively high  $T_{\rm e}$  gradient region appeared in the mid radius region at the timing of the HIGP stopped. However, the dynamic change of the high  $T_{\rm e}$  gradient region during the recovery phase differs from the magnetic field strength. Under the lower magnetic field case less than 1.0T, the high  $T_{\rm e}$  gradient region moves outward. In such the case, the electron ITB has not been formed. In the higher magnetic field case more than 1.28 T, on the other hand, the high  $T_{\rm e}$  gradient region moves inward and finally the electron ITB was formed.

The dependence of the beam absorption power on the magnetic field strength shown in Fig. 7 indicates the increase in the absorbed power with increasing the magnetic field strength, because of the improvement in the drift orbit of the beam ion and the density condition. From the density profile measurement, a shrink of the density profile was confirmed just after the stop of the HIGP fuelling. The experimental results suggest that the onset of the electron ITB formation requires a significant absorbed beam power or energy confinement time during the recovery phase. On the other hand, since the high ion temperature has only observed at B = 1.4 T, further experiments and analysis are required to clarify the transport characteristics between electron and ion.

## 4. DISCUSSIONS

We have conducted a gyrokinetic simulations using GX to investigate the characteristics of the micro-turbulence to discuss the effect contributing to the formation of the high density ITB plasmas. GX is a gyrokinetic turbulence

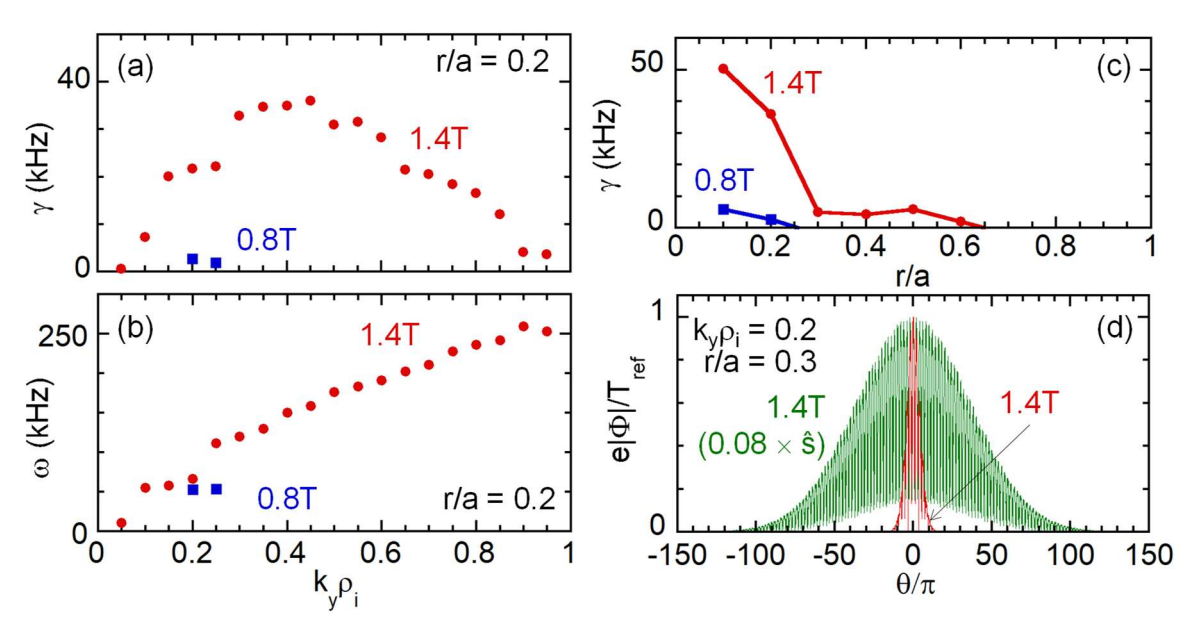


Fig. 8. Comparison of (a) linear growth rate  $\gamma$ , (b) real frequency  $\omega$  as a function of normalized binormal wavenumber  $k_y \rho_i$  at r/a = 0.2 and (c) radial profile of maximum linear growth rate between B = 0.8 and 1.4 T cases. (d) Normalized electrostatic potential  $e|\Phi|/T$  profile of the ITG mode at r/a = 0.3 along with magnetic field line in the case of  $k_y \rho_i = 0.2$  in which the linear growth rate is maximum at the position.

simulation code designed to study microturbulence-driven transport in magnetized plasmas, with applications to both Tokamak and Stellarator/Heliotron devices [34]. This code solves the gyrokinetic equations in a local fluxtube domain, which captures the essential physics of micro-instabilities like ITG and/or trapped-electron-mode (TEM) with reduced computational cost. Since the code is written to fully exploit modern GPU architectures, it has enabled us to make large parameter scans and multi-scale coupling with transport solvers feasible. Figures 8(a) and 8(b) show the linear growth rates  $\gamma$  and the real frequencies  $\omega$  at r/a = 0.2, as a function of the normalized binormal wavenumber  $k_y \rho_i$  in the cases of B = 0.8 and 1.4 T using a Boltzmann electron response. In this simulation, the equilibrium deduced by VMEC fixed boundary condition was used and the input parameters were set based on the experimental observations. At B = 1.4 T, where the electron ITB was observed, the linear growth rate of the ITG mode is unstable in the range of  $0.1 < k_{\rm V}\rho_{\rm i} < 1.0$  with a peak at  $k_{\rm V}\rho_{\rm i} = 0.45$ . This calculation result is consistent to the experimental observation that  $T_c/T_i$  is approximately two. However, higher wavenumber modes should be paid attention to because the magnetic configuration has low magnetic shear, which will be investigated by electromagnetic simulations. The linear growth rate and the wavenumber at which it reaches its maximum are comparable to the gyrokinetic simulations using GKV for the NBI plasmas obtained in Heliotron J with the electron density around  $2x10^{19}$  m<sup>-3</sup> by the normal gas fuelling [35]. For the B = 0.8 case, on the other hand, the linear growth rate is almost stable in the wavenumber space, and it has a peak at  $k_y \rho_i = 0.2$  smaller than that for the B = 1.4 T case. As shown in Fig. 8(c), the radial profile of the maximum linear growth rate at B = 1.4 T has a peak at the core at which the plasma pressure is maximum, while in the case of B = 0.8 T, only in the core region a linear growth rate smaller than that of B = 1.4 T is obtained. In the outer region r/a > 0.3, any positive linear growth rate is not observed. The inconsistency between the experimentally observed heat transport coefficient and the linear growth rate indicates that the importance in the nonlinear effect of the microturbulence to interpret the reduction in the heat transport in the high-density ITB plasmas.

Microturbulence often interacts strongly with magnetic islands, since it modifies local pressure gradients, magnetic shear, and the connectivity of magnetic field lines [6, 7, 36-38]. When turbulent eddies evolve in the distorted magnetic geometry near the magnetic island, their nonlinear self-interaction becomes prominent. Therefore, it is important to investigate the effect of the magnetic island onto the characteristics of the microturbulence, even though the VMEC equilibrium calculation cannot handle the effect of the magnetic islands. We carried out the GX simulations with artificially reduced magnetic shear to take the effects of magnetic islands into account. Figure 8 (d) compares the electrostatic potential profile of the ITG mode along the magnetic field line in case of B = 1.4 T, between the magnetic shear  $\hat{s}$  as determined by the VMEC equilibrium based on the experimental observation and a value of  $\hat{s}$  artificially reduced to 8% of that determined by VMEC. A clear extension in the potential fluctuations of the ITG turbulence for hundreds of poloidal turns is obtained in the case of the small magnetic shear, compared to the original  $\hat{s}$ . Such the extended potential structure of the turbulence

may cause nonlinear interactions with each other. The nonlinear effect, known as eddy self-interaction [36–38], can produce intrinsic torque/stress in the parallel and perpendicular directions to the magnetic field line, which contributes to produce flow shear resulting reduction in the cross-field transport. In fact, we observed a parallel flow velocity shear at the position of the ITB foot as well as the rational surface. The nonlinear interactions described above can be one candidate mechanism for the formation of ITB through the suppression of the heat transport.

In order to clarify the ITB formation mechanism, nonlinear gyrokinetic simulations will be carried out to estimate the magnetic shear and island effects onto the ion/electron heat transport. We are planning to evaluate the intrinsic parallel torque component by comparing the parallel flow velocity measurement to the calculation result using the neoclassical transport analysis [30] with taking the external torque by NBI into account.

#### 5. SUMMARY

In this paper, we demonstrated compatibility between the electron ITB formation and edge density pedestal in the high-density NBI plasmas of Heliotron J. This can be achieved by controlling hydrogen recycling and effective core fuelling with HIGP and by tailoring the rotational transform profile with balanced NB in the low magnetic shear configuration. The experimentally observed plasma performance is summarized as follows: (i) the characteristics of the core electron transport is similar to that of the conventional e-ITB plasmas, (ii) the energy confinement time exceeding the ISS04 scaling law is achieved in the high-density ( $8 \times 10^{19}$  m<sup>-3</sup>) plasmas with the edge density pedestal formation, (iii) the footpoint of the electron ITB coincides with positions at which both the parallel flow velocity shear and the m/n = 7/4 magnetic islands deduced from HINT2 appear, (iv) a different ITB formation mechanism to the CERC transition is expected by the negative neoclassical radial electric field due to the high collisionality and the time scale of the dynamics of the high  $T_c$  gradient region. The GX gyrokinetic simulations indicates the stretch of the ITG mode along with the magnetic field line when the magnetic shear of the Heliotron J configuration becomes low expected at the m/n = 7/4 island position. Although the mechanism behind the ITB formation remains unclear, these experimental and theoretical results suggest a candidate mechanism: intrinsic torque generated by eddy self-interaction produces the flow shear, which may contribute to reduce the heat transport.

## **ACKNOWLEDGEMENTS**

The authors would like to acknowledge the Heliotron J group for their support in conducting the experiments and numerical calculations. The gyrokinetic simulations (GX) were carried out with the help of Drs. I. Abel and M. Landreman in University of Mayland. This work was partly supported by the NIFS Collaborative Research Program (NIFS25KSPM005 and NIFS10KUHL030), Grant-in-Aid for Scientific Research, MEXT (Kiban (B) No. 19H01875 and Kiban (A) 22H00117), and JSPS Core-to-Core Program, A. Advanced Research Networks, PLADyS.

#### REFERENCES

- [1] DING, S., et al., Nature 629 (2024) 555.
- [2] GAROFALO, A.M., et al., Nucl. Fusion 55 (2015) 123025.
- [3] FUKUDA, T., et al., Plasma Phys. Control. Fusion 44 (2002) A341.
- [4] KOIDE, Y., et al., Phys. Rev. Letters 72 (1994) 3662.
- [5] IDA, K., Fujita, T., Plasma Phys. Control. Fusion 60 (2018) 033001.
- [6] GIANNATALE, G.D., Plasma Phys. Control. Fusion 67 (2025) 075008.
- [7] ISHIZAWA, A., et al., Phys. Rev. Letters 123 (2019) 025003.
- [8] MINAMI, T., et al., Plasma Phys. Control. Fusion 44 (2002) A197.
- [9] MINAMI T., et al., Plasma Phys. Control. Fusion 46 (2004) A285.
- [10] MINAMI T., et al., Nucl. Fusion 44 (2004) 342.
- [11] YOKOYAMA, M., et al., Nucl. Fusion 47 (2007) 1213.
- [12] VELASCO, J.L., et al., Nucl. Fusion 48 (2008) 065008.
- [13] OSAKABE, M., et al., Nucl. Fusion 62 (2022) 042019.
- [14] TAKAHASHI, H., et al., Nucl. Fusion 58 (2018) 106028.

#### IAEA-CN-316/INDICO ID

[Right hand page running head is the paper number in Times New Roman 8 point bold capitals, centred]

- [15] BOZHENKOV, S.A., et al., Nucl. Fusion 60 (2020) 066011.
- [16] OKAMURA, S. et al., Nucl. Fusion 45 (2005) 863.
- [17] MINAMI T., et al., Plasma Fusion Res. 1 (2006) 032.
- [18] WANG, C., et al., Plasma Phys. Control. Fusion 66 (2024) 022001.
- [19] MIZUUCHI, T., et al., J. Nucl. Mater. 438 (2013) S453.
- [20] KOBAYASHI, S. et al., Proc of 26th IAEA Fusion Energy Conf (2016) EX/P8-17.
- [21] LU, X.X., et al., Plasma Fusion Res. 13 (2018) 1202077.
- [22] KOBAYASHI, S., et al., Nucl. Fusion 61 (2021) 116009.
- [23] KOBAYASHI, S., et al., Plasma Phys. Control. Fusion 62 (2020) 065009.
- [24] KOBAYASHI, S., et al., Nucl. Fusion 51 (2011) 062002.
- [25] OGIHARA, K., et al., Sci. Rep 15 (2025) 16503.
- [26] MURAKAMI, S., Fusion Technol. 27 (1995) 256.
- [27] YAMADA, H., et al., Proc. 31st EPS Conf. on Contr. on Fusion and Plasma Phys. ECA Vol. 28G, P-5 099 (2004).
- [28] LEE, H., et al., Plasma Phys. Control. Fusion 55 (2013) 035012.
- [29] SEKI, R., et al., Plasma Fusion Res. 6 (2011) 2402081.
- [30] NISHIOKA, K., et al., Phys. Plasmas 23 (2016) 032511.
- [31] SPONG, D.A., et al., Phys. Plasmas 12 (2005) 056114.
- [32] NAGAOKA. K., et al., Nucl. Fusion 51 (2011) 083022.
- [33] KENMOCHI, N., et al., Plasma Phys. Control. Fusion 59 (2017) 055013.
- [34] MANDELL, N.R., et al., J. Plasma Phys. 90 (2024) 905900402.
- [35] ISHIZAWA A., et al., Nucl. Fusion 57 (2017) 066010.
- [36] VOLČOKAS, A, et al., Nucl. Fusion 63 (2022) 014003.
- [37] VOLČOKAS, A., et al., Plasma Phys. Control. Fusion 67 (2024) 015001.
- [38] VOLČOKAS, A., et al., Plasma Phys. Control. Fusion 67 (2024) 015002.